Hindawi Publishing Corporation
Journal of Nanomaterials
Volume 2015, Article ID 538954, 15 pages
http://dx.doi.org/10.1155/2015/538954

Review Article

Metal-Insulator Phase Transition in Quasi-One-Dimensional VO_2 Structures

Woong-Ki Hong,[1] SeungNam Cha,[2] Jung Inn Sohn,[2] and Jong Min Kim[2]

[1] *Jeonju Center, Korea Basic Science Institute, Jeonju, Jeollabuk-do 561-180, Republic of Korea*
[2] *Department of Engineering Science, University of Oxford, Oxford OX1 3PJ, UK*

Correspondence should be addressed to Woong-Ki Hong; wkh27@kbsi.re.kr and Jung Inn Sohn; junginn.sohn@eng.ox.ac.uk

Received 15 January 2015; Accepted 16 March 2015

Academic Editor: Chetna Dhand

The metal-insulator transition (MIT) in strongly correlated oxides has attracted considerable attention from both theoretical and experimental researchers. Among the strongly correlated oxides, vanadium dioxide (VO_2) has been extensively studied in the last decade because of a sharp, reversible change in its optical, electrical, and magnetic properties at approximately 341 K, which would be possible and promising to develop functional devices with advanced technology by utilizing MITs. However, taking the step towards successful commercialization requires the comprehensive understanding of MIT mechanisms, enabling us to manipulate the nature of transitions. In this regard, recently, quasi-one-dimensional (quasi-1D) VO_2 structures have been intensively investigated due to their attractive geometry and unique physical properties to observe new aspects of transitions compared with their bulk counterparts. Thus, in this review, we will address recent research progress in the development of various approaches for the modification of MITs in quasi-1D VO_2 structures. Furthermore, we will review recent studies on realizing novel functional devices based on quasi-1D VO_2 structures for a wide range of applications, such as a gas sensor, a flexible strain sensor, an electrical switch, a thermal memory, and a nonvolatile electrical memory with multiple resistance.

1. Introduction

Strongly correlated oxide materials undergoing reversible transitions between metallic and insulating states have been gaining interest because of their unique physical properties coupled with various phase transitions as well as their potential for application in electronic devices, thermochromic devices, optical and holographic devices, sensors, actuators, and power meter or thermometer [1–22]. However, in spite of the attractive features of strongly correlated systems associated with metal-insulator transitions (MITs), it has been difficult to move forward towards commercially viable industrial applications. These problems have been mainly associated with the lack of not only comprehensive and fundamental understandings of underlying physics accounting for the precise transition mechanism but also appropriate materials and technology. Therefore, recent research has been focused on MITs in single-domain nanostructures due to their unique geometry and favorable domain size, providing a simple and homogeneous system to explore the intrinsic property of individual phases or single-domain phenomena, which are obscured in bulk samples.

Among the strongly correlated materials, vanadium dioxide (VO_2) is the most interesting because of its first-order MIT near easily accessible temperature (approximately 341 K) that is accompanied by a structural phase transition (SPT) from a low-temperature monoclinic phase (M1, $P2_1/c$) to a high-temperature rutile phase (R, $P4_2/mnm$) [3, 4, 21]. Although there have been continued debates on whether the MIT in VO_2 is usually driven by strong electron-electron correlations associated with the Mott transition or electron-phonon interactions associated with the Peierls transition, VO_2 has attracted significant attention as a potential candidate for electronic and photonic devices based on MITs because of its tunable electrical and optical switching features at ultrafast time scale [1–23]. In particular, quasi-one-dimensional (quasi-1D) VO_2 structures can provide new opportunities to explore, understand, and ultimately engineer

MIT properties for developing novel functional devices as they exhibit significantly different properties compared with their bulk counterparts due to surface effects and unique dimensionality [3, 4, 21]. In addition, phase transitions in quasi-1D VO_2 structures can be significantly affected and tuned by doping, interfacial stress, external stress, and stoichiometry and/or defects. Accordingly, considerable and extensive efforts have been recently devoted to the understanding of MIT behavior and fundamental mechanisms in quasi-1D VO_2 structures and their practical applications, such as sensors, switching, and memory devices [24–44]. In this review, therefore, we will first describe the basic crystal and electronic structures of VO_2 related to metallic and insulating phases and the representative growth method of quasi-1D VO_2 structures based on the vapor phase transport process. Then, we will review recent research carried out on the quasi-1D VO_2 structures, particularly focusing on the development of various approaches for tunable MITs by doping, surface stress, external stress, and stoichiometry and/or defects. Lastly, we will discuss recent functional applications based on quasi-1D VO_2 structures for gas and strain sensing, electrical switching, and thermal and nonvolatile electrical memory technologies.

2. Crystal and Molecular Orbital Structures of VO_2

VO_2 exhibits at least four different phases: the monoclinic M1, triclinic T, monoclinic M2, and rutile R phases. The electronic metal-insulator phase transition in VO_2 is coupled with a SPT from a high-temperature metallic rutile (R) phase ($P4_2/mnm$ space group) to a low-temperature insulating monoclinic (M1) phase ($P2_1/c$ space group) at a temperature of approximately 341 K (Figure 1) [3, 4, 22, 23]. All V atoms are equally spaced along linear chains of VO_6 octahedra parallel to the crystallographic c-axis (c_R) with V–V distances of 2.86 Å in the R phase, as shown in Figure 1(a). During the MIT from a metallic R phase to an insulating M1 phase, two distinctive sets of V–V bond distances are observed at 2.65 and 3.12 Å for the monoclinic M1 phase due to the pairing and tilting of VO_6 octahedra with respect to the rutile c-axis, c_R (Figure 1(a)) [22, 23]. Another monoclinic phase (M2, C2/m space group) has two types of V chains consisting of equal-spaced tilted V chains and paired V chains. Recently, M2 phases in VO_2 micro/nanocrystals were reported to exist in the M1 and the R phase through stabilization by tensile stresses resulting from VO_2 crystals bent or clamped to the substrate as well as stoichiometric defects due to the variation of lattice constants [38, 39, 45–47]. The insulating character of the metastable M2 phase has been described as a Mott insulator driven by electron-electron correlation [3, 4, 21]. The T phase is a transitional phase between the M1 and M2 phases [3, 21, 39].

The SPT in VO_2 is accompanied by a change of the electronic structures in the metallic and insulating states which was described in terms of molecular orbital theory [22, 23, 48, 49]. In the high-temperature metallic state (as shown schematically in the left side of Figure 1(b)), the density of states at E_F is formed from a mixture of the half-filled $d\|$ band oriented along the c_R and antibonding π^* band. Across the MIT, the dimerization of the V ions along the c_R and the tilting of the VO_6 octahedra splits the $d\|$ bands that mediate V–V bonds into a bonding ($d\|$) combination and an antibonding ($d\|^*$ and π^*) combination. This results in the orbital polarization with the bonding $d\|$ band being fully occupied and the $d\|^*$ and π^* being empty.

3. Growth of Quasi-1D VO_2 Structures

In recent years, considerable efforts have been made to grow single-crystalline VO_2 nanobeams or nanowires using a vapor phase transport method because of difficulties of growth associated with the presence of various competing vanadium oxide phases [24–29]. It has been reported that the growth characteristics, morphology and composition features, and density of VO_2 nanostructures are significantly affected by growth parameters such as temperature, gas flow rate, oxygen partial pressure, precursor deposition rate, and crystallographic plane of growth substrates [24–29]. To explain this phenomenon, Kim et al. [24] reported that liquid droplets of V_2O_5 nucleate initially and then these droplets may become nucleation sites for the growth of VO_2 nanowires. Strelcov et al. [25] conducted direct in situ optical and photoelectron emission microscopy observations of the nucleation and growth of VO_2 nanostructures using thermal transport of V_2O_5 precursor in a vacuum or in an inert gas environment. They observed the coexistence and transformation of the intermediate oxide phases and morphologies during nanostructure reductive growth, as shown in Figure 2(a). In Figure 2(a), the temperature-composition phase diagram shows that vanadium oxides can have a variety of stoichiometries due to multiple oxidation states of vanadium in which the stoichiometries are mutually transformable at specific temperatures and oxygen partial pressures. Kim and Lauhon [26] also studied controlled morphology, density, and site-specificity of VO_2 nanobeams using a two-step vapor transport method. As seen in Figure 2(b), they observed three distinctive morphologies of VO_2 nanostructures, such as nanoparticles, nanowires, and nanosheets, depending on local source supersaturation and temperature. In addition, as shown in Figures 2(c)–2(f), some previous studies have also shown that VO_2 nanowires can form on various substrate surfaces and display either in-plane or out-of-plane growth, depending on the crystallographic orientation and lattice mismatch of growth substrates as well as the temperature of the reactor [27–29].

4. Stimuli Effects on MITs in Quasi-1D VO_2 Structures

4.1. Influence of Doping on MIT. The ability to incorporate transition metal ions into quasi-1D VO_2 structures, which can play a key role in determining their MIT properties, is extremely important for a variety of applications such as optical switches, smart window coating, Mott transistors, memristors, sensors, and thermal actuators [30–32, 40–44].

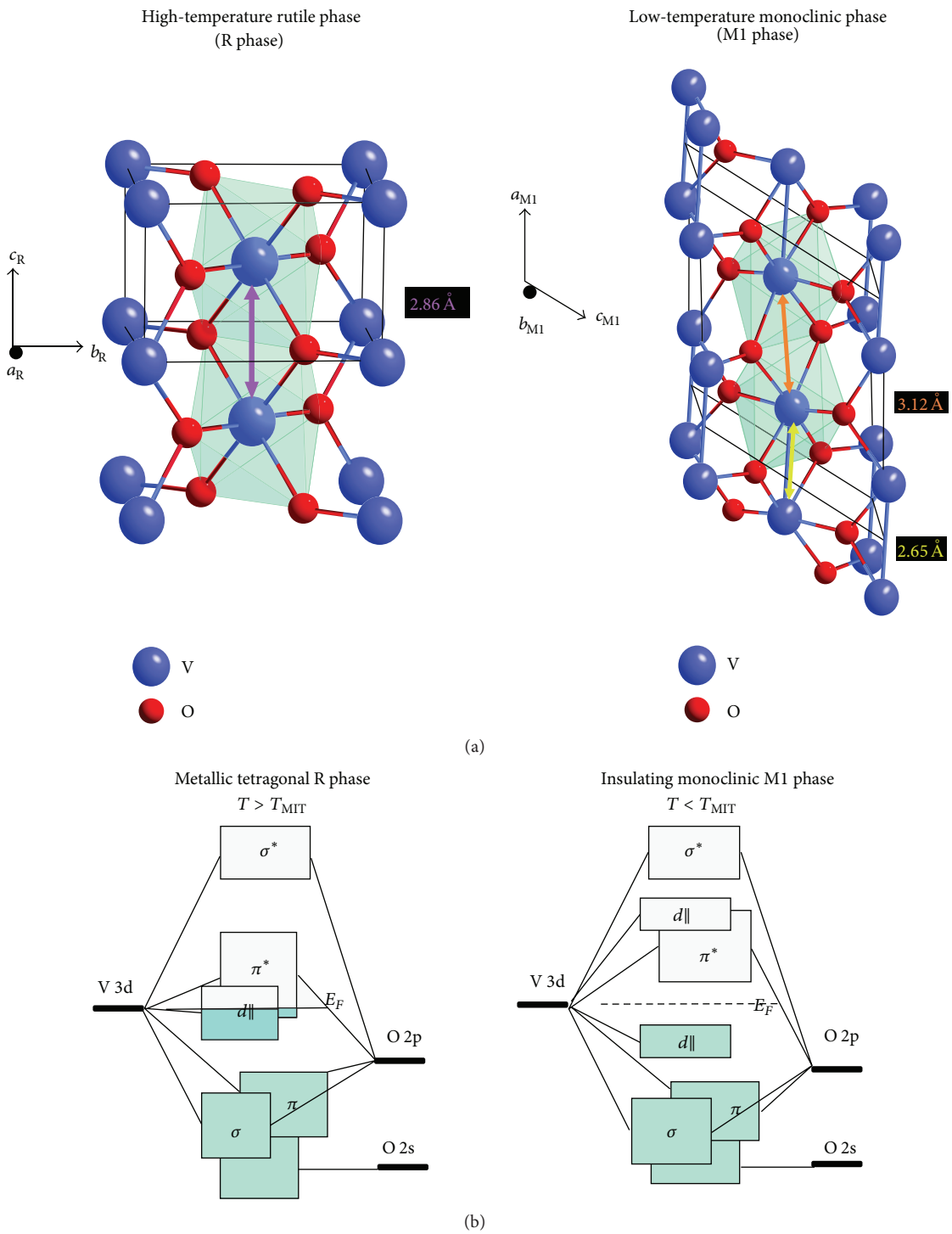

FIGURE 1: (a) The crystal structures of the high-temperature tetragonal rutile (R, space group $P4_2/mnm$) and low-temperature monoclinic (M1, space group $P2_1/c$) phases of VO_2, with the equivalent direction of $a_{M1} = 2c_R$. V–V distances are highlighted: the R phase with regular VO_6 octahedron exhibits uniform V–V distances of 2.86 Å and the M1 phase with distorted VO_6 octahedron exhibits alternating V–V distances of 2.65 and 3.12 Å. (b) A schematic diagram of the molecular orbital structures of the M1 and R phases of VO_2 (left side: the undistorted metallic phase of VO_2, right side: the distorted insulating phase of VO_2). Panels (a) and (b) adapted with permission from [23] and [22], respectively.

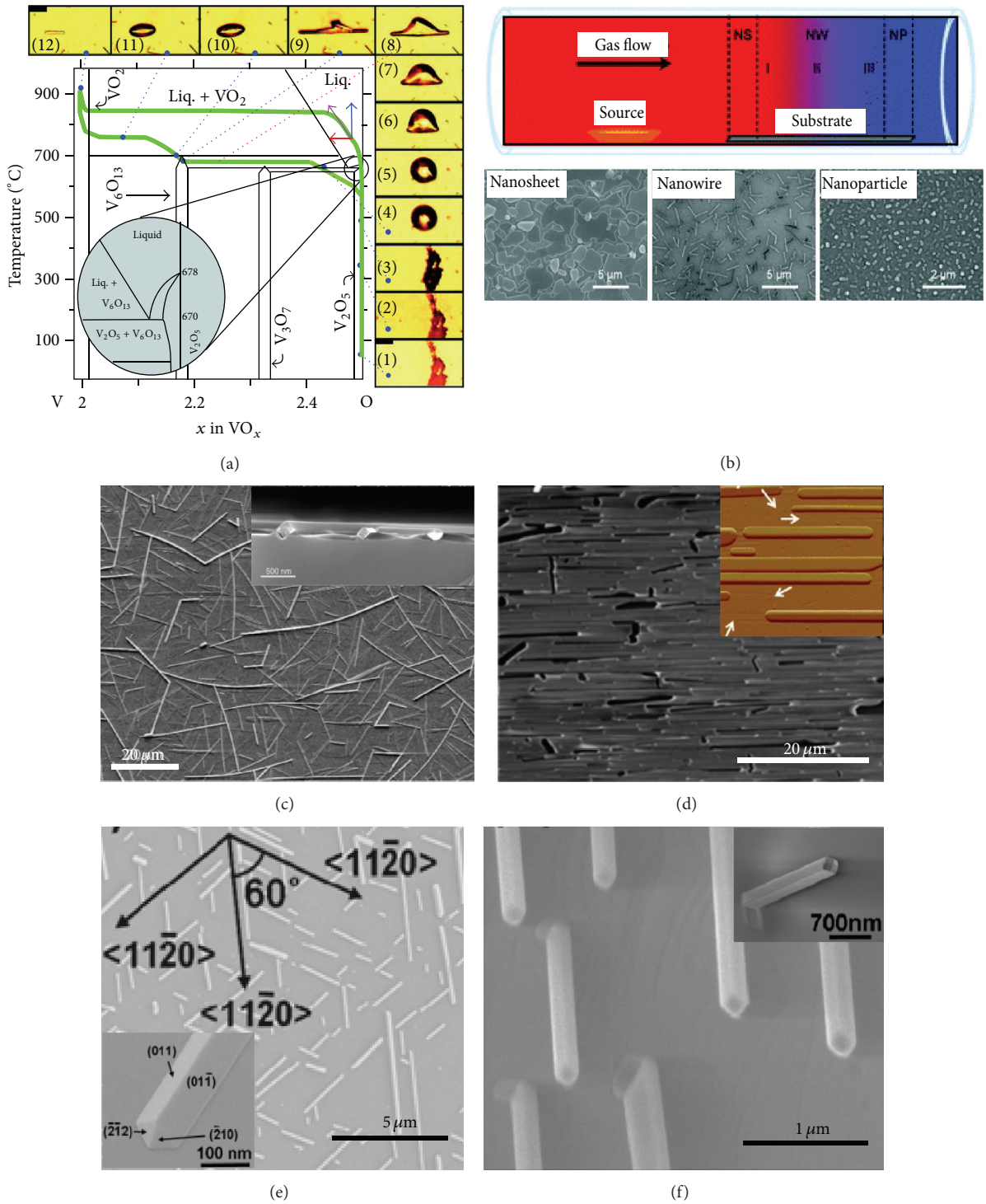

FIGURE 2: (a) Temperature-composition phase diagram. (b) Schematic of the tube furnace reactor. Temperature of the reactor is illustrated by red (hot) and blue (cold) colors. Representative morphologies of the growth product observed in accordance with source vapor pressure include nanosheets (left), nanowires (middle), and nanoparticles (right). SEM images of VO_2 nanowires as grown on (c) Si_3N_4, (d) quartz, and (e) c-cut sapphire and r-cut sapphire substrates. The inset in (c) shows SEM image showing the cross sections of three VO_2 nanowires embedded in a Si_3N_4 surface. The inset in (d) shows AFM image of VO_2 nanowires. The inset in (f) shows a high-magnification SEM image, showing the morphology of a VO_2 nanowire with well-defined surfaces at both a tip and a side. Panels (a–f) adapted with permission from [25–29], respectively.

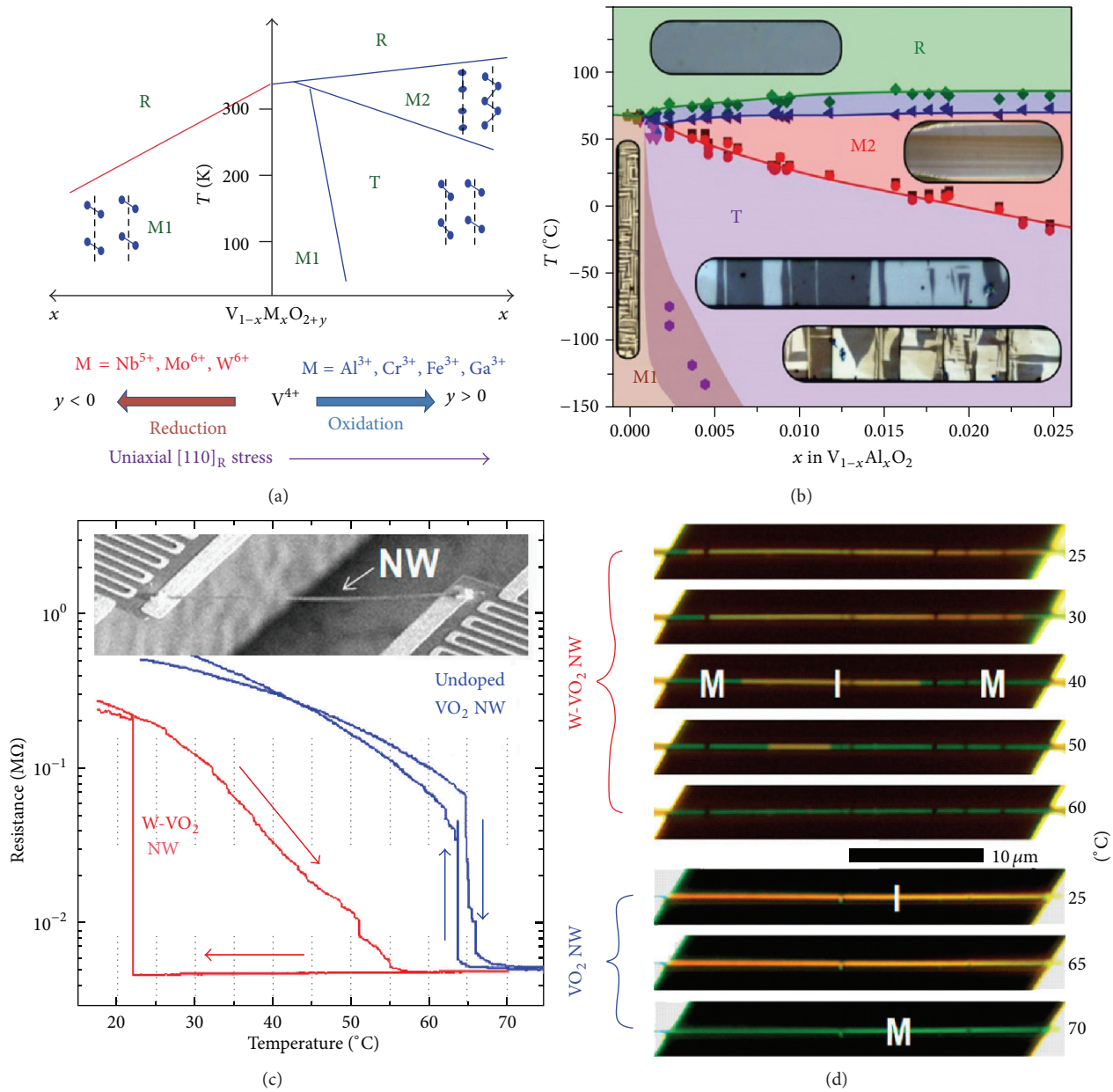

Figure 3: (a) Schematics of temperature-composition phase diagram. (b) Experimental temperature-composition phase diagram for free-standing Al-doped VO_2 nanostructures. (c) Temperature dependence of resistance of a W-doped nanobeam and an undoped VO_2 nanobeam. The inset shows a SEM image of a VO_2 nanobeam on suspended pads. (d) Optical images of the W-doped VO_2 nanobeam device (upper panel) and the undoped VO_2 nanobeam device (lower panel) at various temperatures during heating. The metallic and insulating phases are denoted as M and I, respectively. Panels (a-b) and (c-d) adapted with permission from [30] and [31], respectively.

Figures 3(a) and 3(b) show that the doping of metal ions has a profound influence on the phase transition behavior and transition temperatures of VO_2. It has been reported that the substitution of V^{4+} ions with metal-ion dopants of higher oxidation states, such as W^{6+}, Nb^{5+}, and Mo^{6+}, lowers the transition temperature (T_{MIT}), which is identical to reduction of the V^{4+} ions. In contrast, metal-ion dopants of lower oxidation states, such as Cr^{3+}, Al^{3+}, Fe^{3+}, and Ga^{3+}, stabilize the M2 and T phases of VO_2 at room temperature [30], which is identical to oxidation of the V^{4+} ions. A schematic diagram (Figure 3(a)) shows mutual transformations of VO_2 phases as a function of reduction and oxidation induced by metal-ion dopants. Furthermore, Strelcov et al. [30] have recently demonstrated a practical synthesis procedure for stabilization of the M2 phase at ambient conditions *via* doping metal ions, which can open a way for realization of a purely electronic Mott transition field-effect transistor without an accompanying structural transition. As shown in Figure 3(b),

the authors also produced high-quality uniformly doped single-crystalline structure and demonstrated a temperature-doping level phase diagram in the temperature range close to the ambient conditions by doping aluminum (Al) into VO_2 nanostructures during the growth in which the doping level was varied from zero to $x = 0.025$. In addition, Lee et al. [31] also demonstrated the axially graded-tungsten-(W-) doped VO_2 nanowires and measured resistance (R)-temperature (T) curves of the graded-W-doped and undoped VO_2 nanowires, as shown in Figure 3(c). The undoped VO_2 nanowire shows an abrupt resistance change at 67°C, whereas resistance of the graded-W-doped VO_2 nanowire decreases gradually from room temperature to 60°C without the abrupt resistance change. As shown in Figure 3(d), with the increase in temperature, the metallic phase grows out of the two ends of the W-doped nanowire, followed by a progressive invasion into the insulating phase toward the middle of the W-doped nanowire, and the W-doped nanowire entirely turns into a single metallic phase at 55–60°C compared with the undoped VO_2 nanowire.

Although the doping of metal ions into vanadium oxides is usually regarded as the effective way to control the electron concentration, this process is not reversible. Recently, Wei et al. [32] demonstrated that hydrogen doping into VO_2 is completely reversible process and that the MIT in VO_2 nanostructures can be strongly modified by doping with atomic hydrogen using the catalytic spillover method, which results in the electronic phase transition (i.e., the Mott transition). The authors also demonstrated that the MIT accompanied by a structural phase transition could be reversibly modified by hydrogen doping using a catalytic spillover method [32]. Figures 4(a) and 4(b) show electrical resistivities and structural phases before and after the hydrogen doping of VO_2 microcrystals. In Figure 4(a), the two-terminal device made from an as-grown VO_2 microcrystal shows thermally activated conduction exhibiting an energy gap close to 0.6 eV (black curve). The two-terminal device that baked in flushing hydrogen gas at 150°C for 20 min shows an energy gap close to 0.2 eV (green curve). The energy gap of the device after further baking at 180°C for 20 min (red curve) is nearly zero. The device after annealing at 190°C for 20 min eventually stabilized in the metallic state with a characteristic negative slope (purple curve). The two-terminal device that was annealed in air at 250°C for 20 min recovered the original phase transition and temperature dependence (blue curve). As shown in the SEM images of Figure 4(b), the VO_2 nanobeam becomes straight after hydrogen doping to the fully metallic state, indicating that the fully hydrogen-doped nanobeam has a shorter lattice constant than a monoclinic as-grown VO_2 microcrystal. This is also well supported by the optical microscopy images of a VO_2 microcrystal before and after hydrogen doping.

4.2. Influence of Surface Stress on MIT. The surface stress, affecting the lattice structure and relative stability of competing phases, plays an important role in determining the phase state of VO_2 micro/nanostructures [33–35, 50]. In particular, the surface stresses associated with the interaction between a nanobeam and a substrate for VO_2 nanobeams with and without epitaxial interfaces significantly affect the MIT behavior in VO_2 nanobeams, the spontaneous formation of metal-insulator domains, and the spatial phase transitions as well as the formation and stabilization of an M2 phase. For example, as shown in Figure 5(a), VO_2 nanobeams lying on a SiO_2 substrate (referred to as on-substrate VO_2 nanobeams) without metal contacts exhibit the spontaneous formation of alternating metal-insulator domains along the nanobeam length, resulting from an adhesive interaction between the nanobeam and the substrate leading to a coherent uniaxial strain on the nanobeam [33]. Figure 5(b) shows that the electrical resistance of devices made from the on-substrate VO_2 nanobeams changes in many discrete steps over a much wider temperature range during the heating and cooling cycles [33].

Sohn et al. [34] demonstrated how the epitaxial interface stress affects the phase transition behavior in VO_2 nanobeams epitaxially grown on c-cut sapphire. Figure 6(a) shows the temperature-dependent evolution of X-ray diffraction (XRD) spectra related to the (011)M1 and (020)M1 planes. Contour plots exhibit coexisting characteristics within the temperature region of 54–64°C and 68–80°C for corresponding (011)M1 and (020)M1 planes (marked by yellow dotted lines), respectively. In particular, in Figure 6(a), the peak corresponding to the $(\bar{2}01)$ plane of M2 is broader than that expected at low temperature and its peak position shifts slightly upward compared to the value of an M2 phase in VO_2 nanobeams without the epitaxial interface. A SPT in the (011) plane occurs from 54°C, whereas a peak of the (020) plane splits into two peaks of (200)R and (002)M2 planes corresponding to the (020) plane of an M1 phase from 68°C, indicating the coexistence of M2 and R phases. Figure 6(b) shows temperature-dependent Raman and XRD spectra for VO_2 nanobeams [35]. The temperature-dependent Raman spectra, which are obtained from the straight part (marked by A in the upper inset) and bent part (marked by B in the lower inset) of a bent VO_2 nanobeam on a c-cut sapphire substrate, demonstrate the stress-induced structural transitions and the coexistence of three distinct M1, M2, and R phases. The evolution of Raman spectra of the straight region of a nanobeam (A) exhibits direct structural changes from M1 to M2 phases, whereas those of the bent part of a nanobeam (B) display coexistence of both M1 and M2 phases with increasing temperature and peaks associated with only M1 and M2 phases are observed even at room temperature. The XRD spectra from ensembles of epitaxially grown VO_2 nanobeams were obtained at the temperature range of 6–303 K during the cooling process. At 303 K, peaks of (011)M1 and corresponding $(\bar{2}01)$M2 planes coexist and the coexisting region exists down to 50 K through the direct transformation of the remaining M2 phase to an M1 phase.

4.3. Influence of External Stress on MIT. The control of the domain structure and phase transitions through external stress in VO_2 could lead not only to deeply understanding the correlated electron materials but also to providing a novel way to control their electrical and optical properties

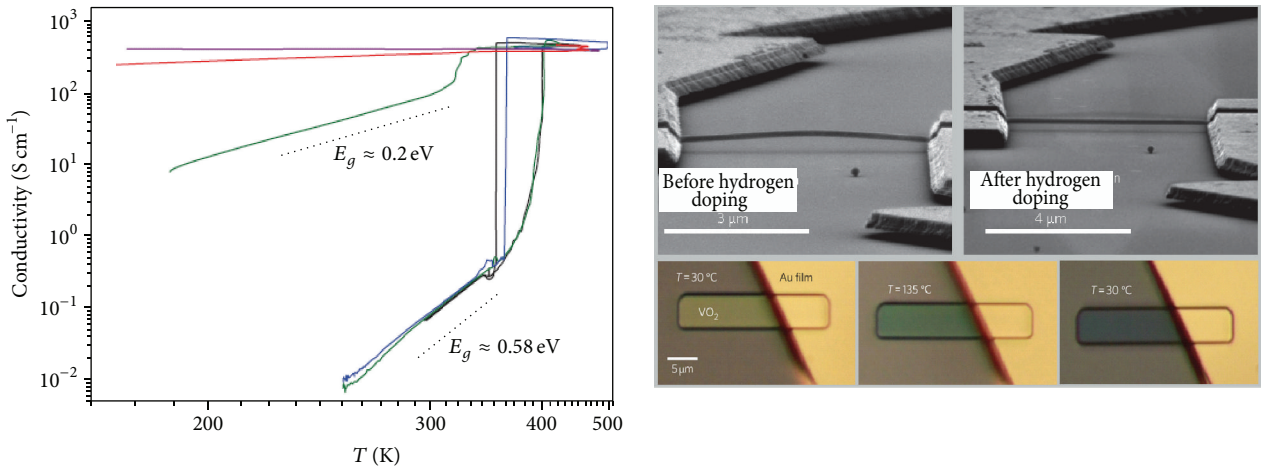

(a) (b)

Figure 4: (a) Conductivity versus temperature (T) for a suspended VO_2 nanobeam device. (b) SEM images showing suspended VO_2 nanobeam devices before and after hydrogen. Optical images of VO_2 microcrystals with thicknesses of ~300 nm on a silicon oxide substrate taken at 30°C (lower left panel) and 135°C (lower middle panel) and at 30°C (lower right panel) after hydrogen doping. The brighter region is a 20 nm gold film deposited to cover parts of the crystals. The scale bar in the lower right panel of (b) applies to all three images. Panels (a) and (b) adapted with permission from [32].

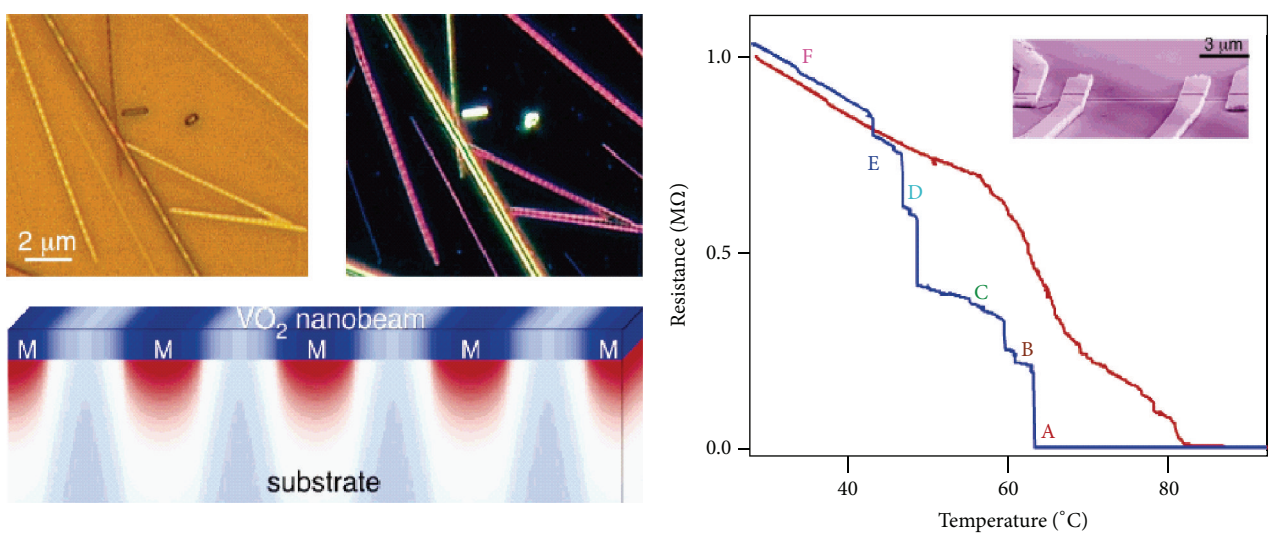

(a) (b)

Figure 5: (a) Bright (upper left) and dark (upper right) field optical images of VO_2 nanobeams grown on a SiO_2 surface at $T = 100$°C during cooling in air. The schematic diagram shows the periodic domain pattern of a VO_2 nanobeam strained on the SiO_2 substrate. Blue and red colors correspond to tensile and compressive strains, respectively. "M" denotes metallic phase, and the unlabeled intervening regions are insulating phase. (b) Resistance of an on-substrate VO_2 nanobeam as a function of temperature during a heating cycle (red curve) and a cooling cycle (blue curve). The inset shows a SEM image of the on-substrate VO_2 nanobeam device. Panels (a) and (b) adapted with permission from [33].

for device applications. Recently, the phase transitions and domain dynamics between metallic and insulating phases in single-crystalline qausi-1D VO_2 beams have been explored by introducing the external stress [3, 36, 37, 41, 42, 51]. For example, Cao et al. [36] demonstrated that periodic domains of metallic and insulating phases along single-crystal VO_2 microbeams were nucleated and manipulated by tuning the strain over a wide range of values, as shown in Figure 7. Figure 7(a) shows the evolution of domains of triangular shape along a bent VO_2 microbeam at different temperatures. The bent microbeam was in an insulating phase at room temperature and periodic triangular domains of the metallic phase started to nucleate at the inner edge of the bent region (compressive strain) at elevated temperatures. At a temperature near 341 K, the straight part of the microbeam transformed abruptly to the metallic phase, whereas the bent

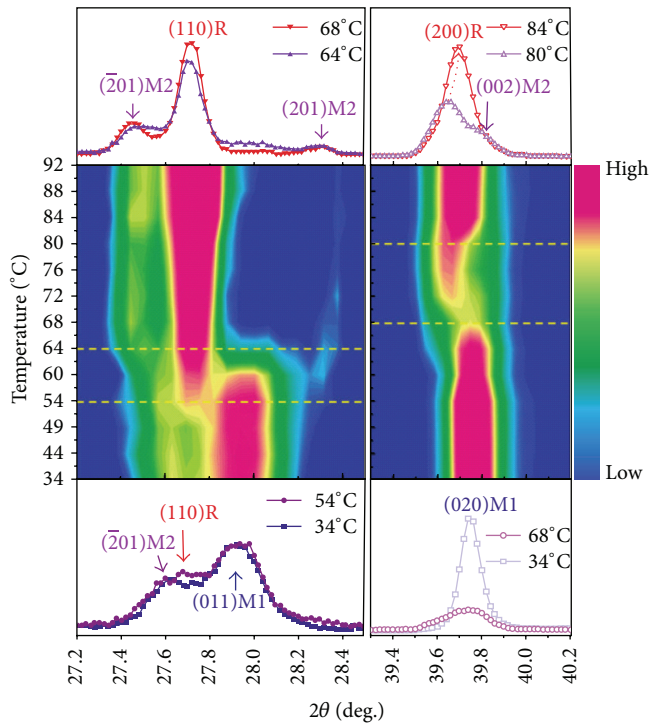

(a)

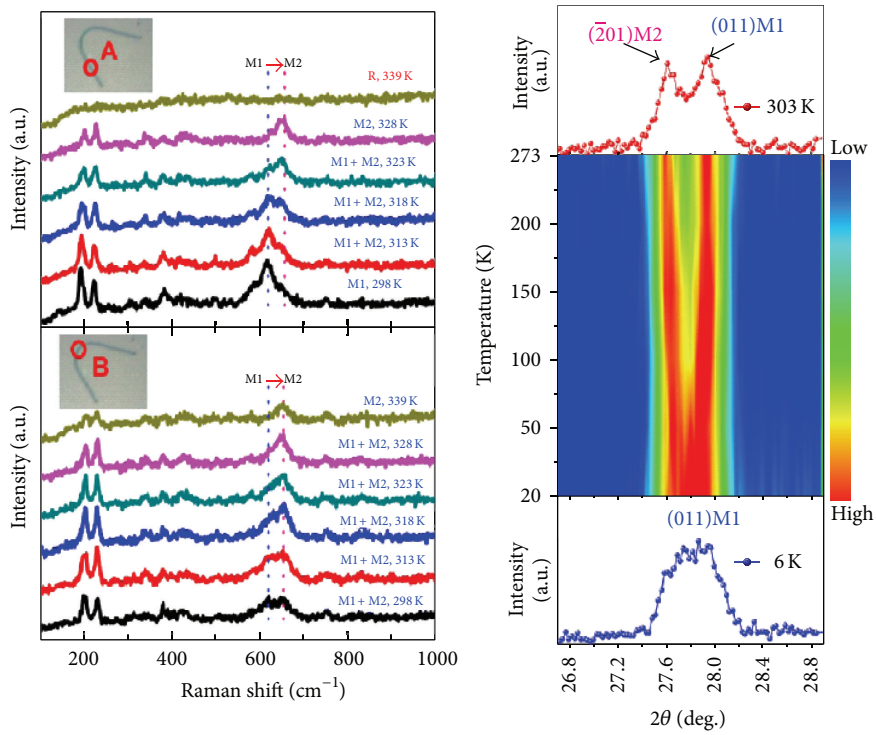

(b)

Figure 6: (a) Temperature dependence of XRD data measured upon heating from VO_2 nanobeams epitaxially grown on a c-cut sapphire. (b) Temperature-dependent Raman spectra obtained from a bent VO_2 nanobeam on a c-cut sapphire substrate (left panel). Temperature dependence of XRD data from ensembles of the VO_2 nanobeams, measured during a cooling cycle from 303 to 6 K (right panel). Panels (a) and (b) adapted with permission from [34] and [35], respectively.

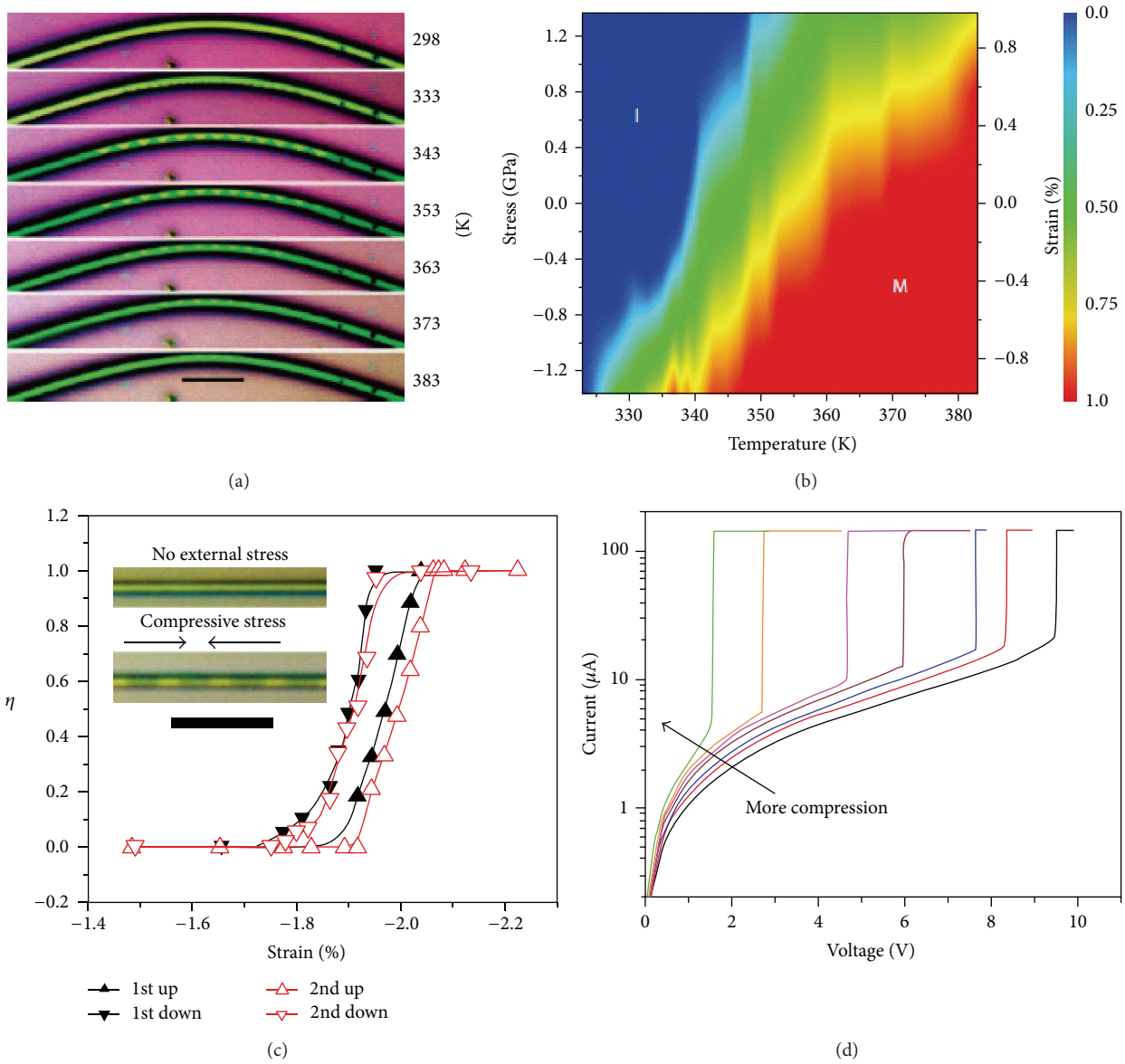

Figure 7: (a) Optical images of an ordered array of triangular metallic (dark regions) and insulating (bright regions) domains nucleated and stabilized by tensile and compressive strains during a heating cycle. (b) A phase diagram as a function of temperature and uniaxial stress or strain. (c) The metallic phase fraction (η) as a function of the total strain. The inset shows representative optical images of metal-insulator domains along a compressive stressed beam. (d) Current-voltage characteristics of a VO_2 beam under different axial compressions at room temperature. The scale bars in (a) and (c) are 10 μm. Panels (a–d) adapted with permission from [36].

part of the microbeam showed a coexistence of domains of the metallic and insulating phases. The uniaxial stress (σ)-temperature (T) phase diagram in Figure 7(b) shows the fraction of the metallic and insulating phases as a function of temperature (x-axis) and uniaxial stress (left y-axis) or strain (right y-axis). In the diagram, the VO_2 phase is a pure metallic phase (metallic phase fraction $\eta = 1$) at high temperatures and high compressive stresses and a pure insulating phase ($\eta = 0$) at low temperatures and high tensile stresses. At intermediate temperatures and stresses, metallic and insulating phases coexisted. Figure 7(c) also shows how the metallic phase fraction (η) changed with external compressive stress along the length of a VO_2 microbeam clamped onto a soft substrate. The uniaxial compression reversibly induces a phase transition between metal ($\eta = 1$) and insulator ($\eta = 0$) at room temperature in the clamped VO_2 microbeams. The microbeam can be self-heated into the metallic phase when the applied bias voltage exceeded a threshold transition voltage and the operation power of the self-heated VO_2 microbeam can be drastically reduced under the uniaxial compression at room temperature. Figure 7(d) shows the experimental observation of a MIT behavior induced by Joule heating under the external compression in the VO_2 microbeam device.

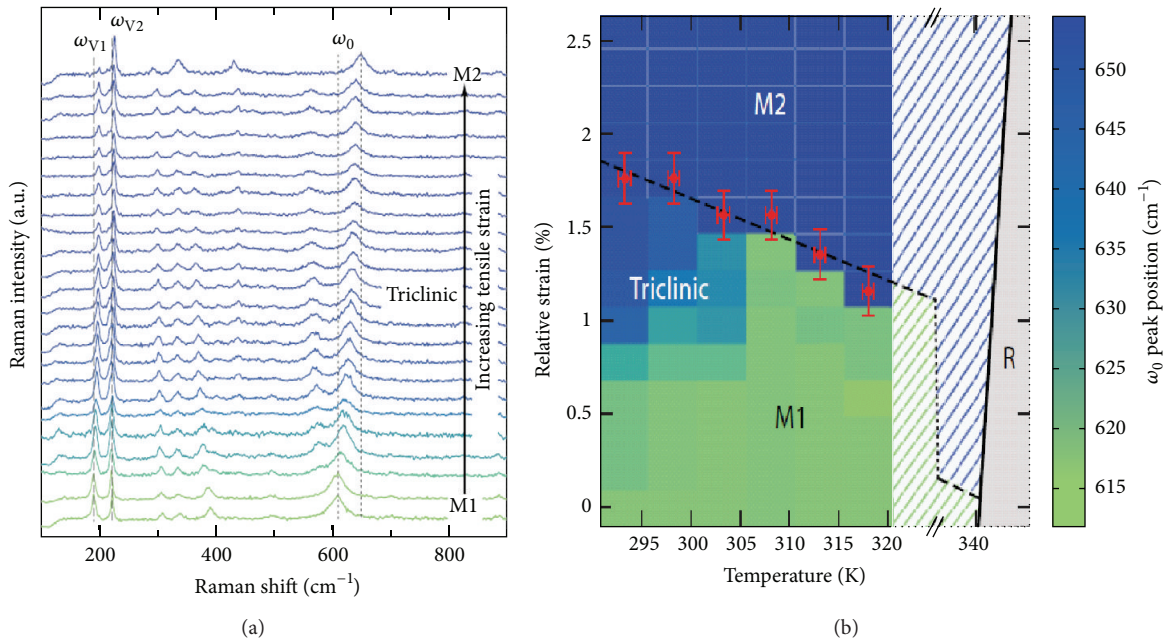

Figure 8: (a) Raman spectra of a VO_2 microcrystal showing the tensile strain-dependent evolution of structural phase transitions at room temperature. (b) A Raman frequency map of strain-temperature phase diagram of the insulating phases of the VO_2 microcrystal represented via the ω_0 phonon frequency shift. Panels (a) and (b) adapted with permission from [37].

To investigate the influence of external stress on crystallographic phase transition behavior in VO_2 microcrystals, Atkin et al. [37] employed Raman spectroscopy, which is a facile, rapid, and nondestructive tool for studying the phase transition properties of individual nano/microstructures. The authors demonstrated that, with increasing tensile strain, an M1–T–M2 structural phase transition occurs at temperatures below approximately 305 K over a wide range of strain values in an individual, homogeneous VO_2 microbeam subjected to external uniaxial strain, as shown in Figures 8(a) and 8(b). Figure 8(a) shows Raman spectra of a VO_2 microcrystal showing the evolution in phonon modes with increasing tensile strain at room temperature. From these Raman spectra, a Raman frequency map is presented based on the spectral position of ω_0 as a fingerprint for the three different phases (M1, T, and M2 phases) (Figure 8(b)).

4.4. Influence of Stoichiometry and/or Defects on MIT. The MIT properties of VO_2 are significantly affected by stoichiometry and/or defects due to the fact that vanadium can exist in multiple valence states such as V^{3+}, V^{4+}, and V^{5+} [38, 39, 52–55]. Recently, Zhang and coworkers [38] investigated the influence of stoichiometry on the structural phase transition in suspended single-crystalline VO_2 nanobeams and established a pseudo-T-δ phase diagram with dimensions of temperature and stoichiometry, as shown in Figure 9(a). The authors also demonstrated that the annealing of nanobeams under vacuum conditions stabilized the rutile phase to temperatures as low as 103 K due to the fact that oxygen deficiency contributed to the enhancement of conductivity, providing direct evidence of substantial electron doping in VO_2 nanobeams (Figure 9(b)). Most recently, Hong et al. [39] demonstrated a morphotropic phase transformation, which is the phase transition due to the compositional variation, in single-crystalline VO_2 nanobeams caused by thermal reduction in a high-pressure hydrogen gas, leading to the stabilization of metallic phases. The authors showed that hydrogen significantly reduced oxygen in the nanobeams with characteristic nonlinear reduction kinetics which depend on the annealing time [39]. Figures 9(c) and 9(d) show that the work function and the electrical resistance of the reduced VO_2 nanobeams follow a similar trend to the compositional variation due to the oxygen deficiency and related defects. These results imply that the structural properties and the electrical resistivity of VO_2 nanobeams are closely correlated with the compositional stoichiometry and/or defects in the nanobeam.

5. Applications

VO_2 has attracted considerable attention because of a variety of potential applications based on abrupt reversible phase transitions at ultrafast timescales in which the phase transition can be triggered by external perturbations, such as thermal, electrical, or optical perturbations as well as strain [1]. Recently, several efforts have been devoted to the demonstration of potential devices utilizing MITs in VO_2 nanostructures, such as gas sensors, strain sensors, electrical switches, a thermal memory, and electrical memory devices [40–44, 56, 57].

For example, Strelcov et al. [40] demonstrated a novel gas sensing concept based on suspended VO_2 nanowires, as shown in Figure 10(a), in which the transition properties of nanowires strongly depend on the changes in molecular

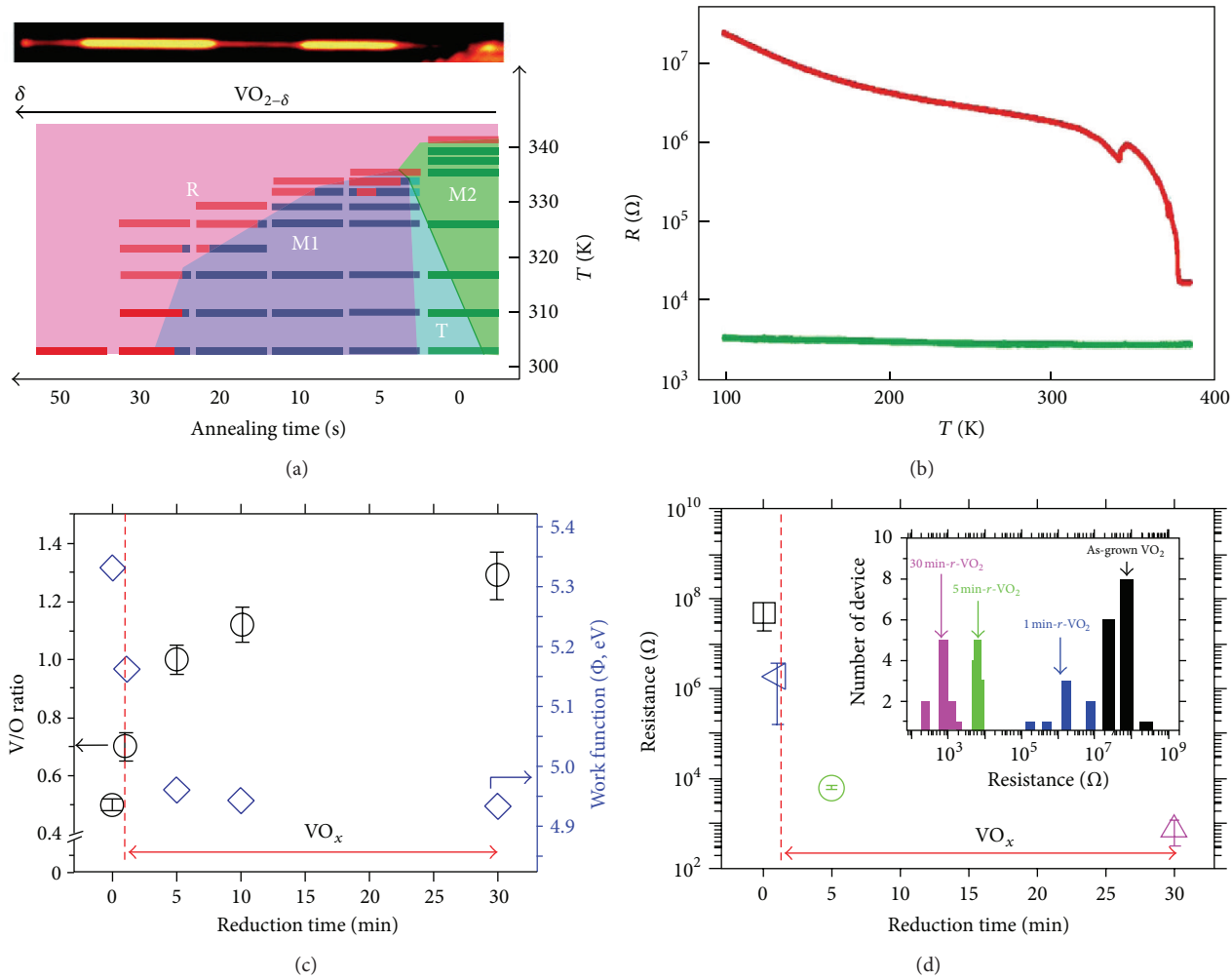

Figure 9: (a) Structural phase maps (temperature versus annealing time). The shaded background demarcates a pseudo-T-δ phase diagram for $VO_{2-\delta}$. Confocal reflectivity at a 532 nm laser source. The brighter (darker) regions correspond to the insulating (metallic) phase (upper image). (b) Resistance versus temperature for as-grown (red) and reduced (green) nanobeams. (c) Change in vanadium (V)/oxygen (O) compositional ratio as a function of reduction time and their corresponding work functions extracted from ultraviolet photoemission spectroscopy measurements. (d) Electrical resistance as a function of the reduction time for the as-grown and reduced VO_2 nanobeams. The inset shows statistical data of the electrical resistance at room temperature for as-grown VO_2 and reduced VO_2 nanobeams for 1, 5, and 30 min at approximately 400°C under the exposure to hydrogen gas. Panels (a-b) and (c-d) adapted with permission from [38] and [39], respectively.

composition, pressure, and temperature of the ambient gas environment. Hu et al. [41] fabricated a flexible strain sensor and a single domain electrical switch based on a VO_2 nanobeam. Figure 10(b) shows the change of the current (I)-voltage (V) behavior solely dependent on the loading strains (compressive and tensile strains) in which the different types of strain lead to the distinct response from the phase transition between M1 and M2 phases. Hu et al. [42] also showed that the self-heated VO_2 nanobeam under the application of a bias voltage that exceeds a threshold transition voltage can be easily switched based on a single domain transition by stretching or compressing the substrate. Figure 10(c) shows a single domain switch based on phase transitions induced by the coupling of self-heating and external strain in a VO_2 nanobeam.

In addition to the sensor and switching device applications, Xie et al. [43] demonstrated a solid-state thermal memory that can store and retain thermal information with high/low (HI/LO) temperature states, as shown in Figure 11(a). In Figure 11(a), HI/LO temperature states of repeated Write HI-Read-Write LO-Read cycles using heating and cooling pulses show the switching performance and repeatability of the thermal memory. Bae et al. [44] also reported a two-terminal memory device based on single VO_2 nanowires that were synthesized by a hydrothermal method, followed by thermal annealing process to form a monoclinic phase (Figure 11(b)). As shown in Figure 11(b), the MIT induced by the Joule heating and the hysteresis behavior leads to the nonlinear R-V characteristic and eventually enables the switchable resistance to be maintained, resulting from

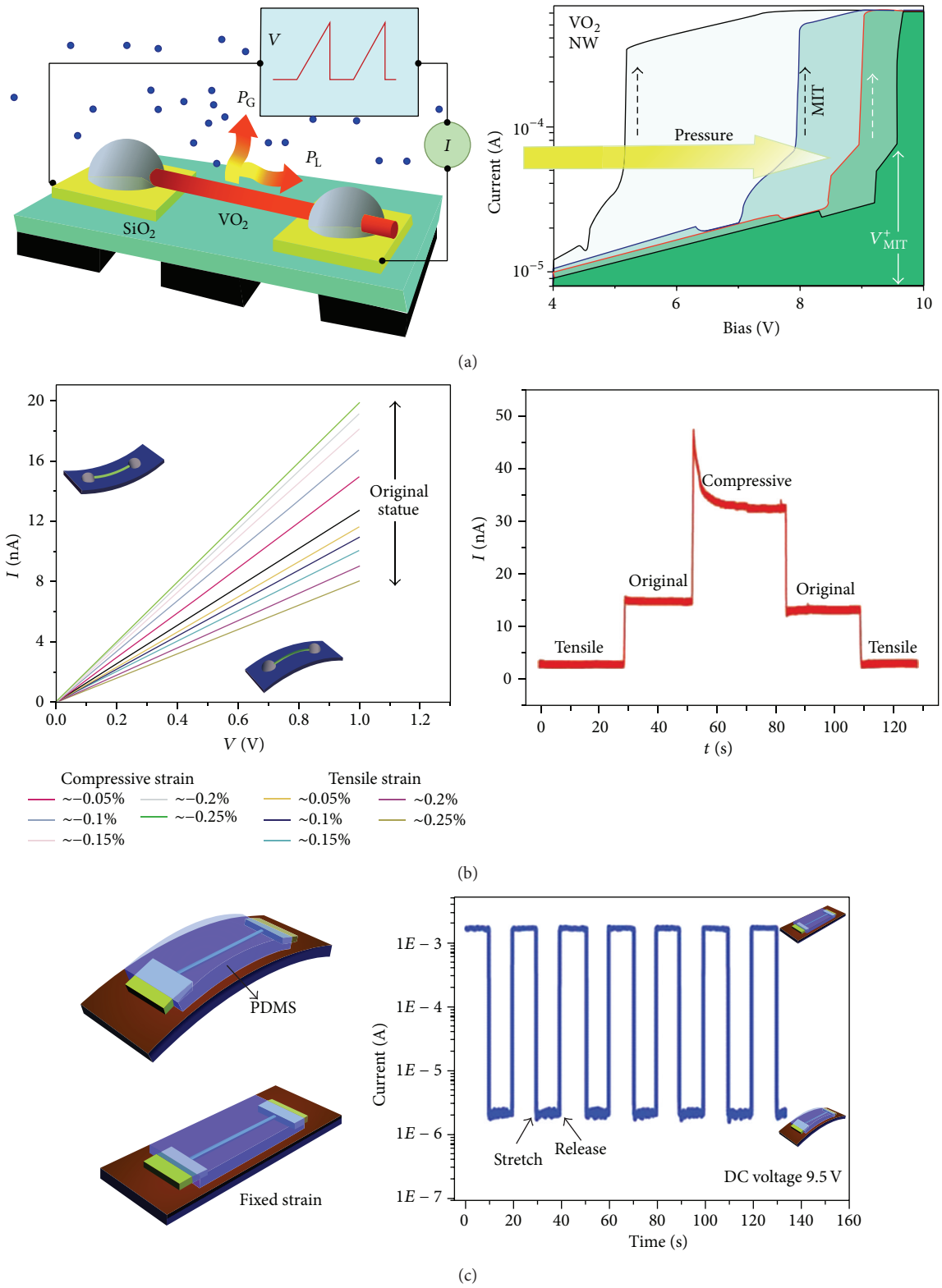

Figure 10: Representative devices utilizing MIT in quasi-1D VO_2 nanostructures. (a) The design and principle of operation of VO_2 nanowire MIT gas sensor (left panel). P_G and P_L indicate heat fluxes dissipating into the gas environment and metal contacts, respectively. Current (I)-bias voltage (V) curves of a self-heated nanowire at different gas pressures showing transition voltages (forward direction) (right panel). (b) I-V curves under different tensile and compressive strains (left panel) and their corresponding response to the strain switch (right panel). (c) Schematic illustration of two-terminal nanobeam device placed on Kapton (left panel). Electrical switch with the strain change based on single domain at DC voltage of 9.5 V (right panel). Panels (a), (b), and (c) adapted with permission from [40, 41] and [42], respectively.

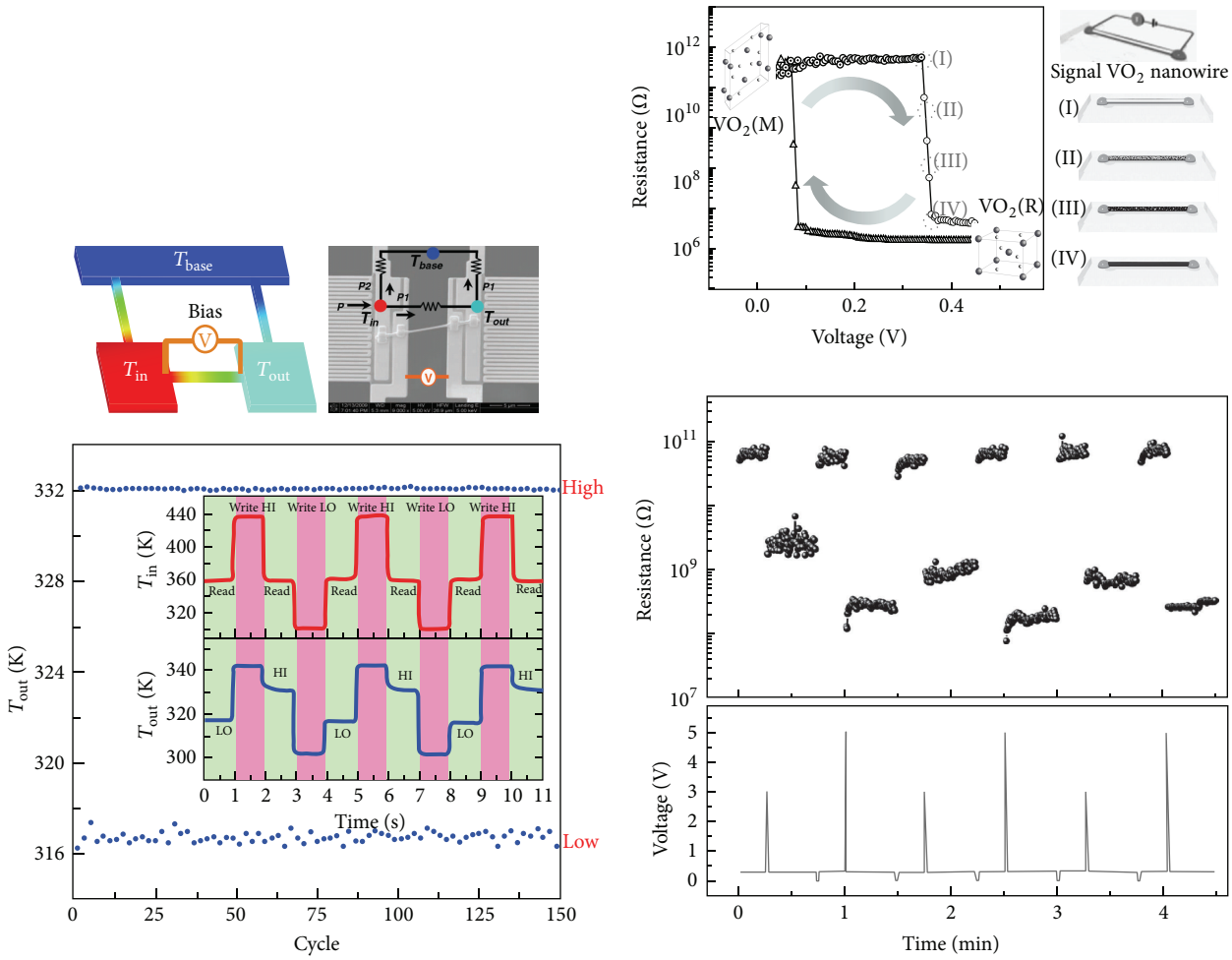

Figure 11: (a) A schematic illustration and a SEM image of a thermal memory device with an individual VO_2 nanobeam connecting the input terminal (T_{in}) and output terminal (T_{out}) (upper panels). High/low (HI/LO) temperature states over 150 repeated cycles by using a one-second heating pulse and a one-second cooling pulse at the input terminal under a voltage bias of 0.04 V (lower panel). The inset shows the process of Write HI-Read-Write LO-Read over three cycles. (b) The resistance (R)-voltage (V) hysteresis curve (upper left panel). Insets show the crystal structures of VO_2 with a monoclinic phase (VO_2(M)) and a rutile phase (VO_2(R)). A schematic of the memory device based on a single VO_2 nanowire showing the gradual change of metallic/insulating phases inside the nanowire at different points marked in the R-V curve (I, II, III, and IV in the upper right panel). Nonvolatile switching property of a single VO_2 nanowire memory device (lower panel). Panels (a) and (b) adapted with permission from [43] and [44], respectively.

the mixed states of metallic and insulating phases during the MIT of the single VO_2 nanowire. The multiple retainable resistances of the single VO_2 nanowire when two different voltage pulses are applied repeatedly show the possibility of nonvolatile memory device utilizing a MIT behavior.

6. Summary

In this review, we first present the basic crystal and molecular orbital structures of VO_2 in metallic and insulating phases and then discuss the growth characteristics of single-crystalline quasi-1D VO_2 structures in terms of their morphology, composition, and density, which can be significantly affected by growth conditions such as temperature, gas flow rate, oxygen partial pressure, precursor deposition rate, and crystallographic plane of growth substrates. Next, we discuss the influence of doping, surface stress, external stress, and stoichiometry and/or defects on various aspects of phase transitions in the quasi-1D VO_2 structures. Lastly, we present snapshots of the research carried out emerging applications of quasi-1D VO_2 structures such as a gas sensor, a flexible strain sensor, an electrical switch, a thermal memory, and a nonvolatile electrical memory. We expect that this review will give insights not only into understanding the basic important aspects of mechanism and properties of quasi-1D VO_2 materials but also into developing practical applications for successful commercialization based on MIT technology.

Conflict of Interests

The authors declare that there is no conflict of interests regarding the publication of this paper.

Acknowledgments

Woong-Ki Hong acknowledges the financial support from the National Research Foundation of Korea (NRF) grant funded by the Korean Government (NRF-2013-R1A1A2009884 and NRF-2014M2B2A4030807). SeungNam Cha, Jung Inn Sohn, and Jong Min Kim acknowledge the support from the International Collaborative Energy Technology R&D Program of the Korea Institute of Energy Technology Evaluation and Planning (KETEP), granted financial resource from the Ministry of Trade, Industry and Energy, Republic of Korea (no. 20128510010080).

References

[1] Z. Yang, C. Ko, and S. Ramanathan, "Oxide electronics utilizing ultrafast metal-insulator transitions," *Annual Review of Materials Research*, vol. 41, pp. 337–367, 2011.

[2] J. Jeong, N. Aetukuri, T. Graf, T. D. Schladt, M. G. Samant, and S. S. P. Parkin, "Suppression of metal-insulator transition in VO_2 by electric field-induced oxygen vacancy formation," *Science*, vol. 339, no. 6126, pp. 1402–1405, 2013.

[3] J. H. Park, J. M. Coy, T. S. Kasirga et al., "Measurement of a solid-state triple point at the metal-insulator transition in VO_2," *Nature*, vol. 500, no. 7463, pp. 431–434, 2013.

[4] T. S. Kasirga, D. Sun, J. H. Park et al., "Photoresponse of a strongly correlated material determined by scanning photocurrent microscopy," *Nature Nanotechnology*, vol. 7, no. 11, pp. 723–727, 2012.

[5] M. M. Qazilbash, M. Brehm, B.-G. Chae et al., "Mott transition in VO_2 revealed by infrared spectroscopy and nano-imaging," *Science*, vol. 318, no. 5857, pp. 1750–1753, 2007.

[6] C. Kübler, H. Ehrke, R. Huber et al., "Coherent structural dynamics and electronic correlations during an ultrafast insulator-to-metal phase transition in VO_2," *Physical Review Letters*, vol. 99, no. 11, Article ID 116401, 2007.

[7] K. Appavoo and R. F. Haglund Jr., "Detecting nanoscale size dependence in VO_2 phase transition using a split-ring resonator metamaterial," *Nano Letters*, vol. 11, no. 3, pp. 1025–1031, 2011.

[8] R. Lopez, L. A. Boatner, T. E. Haynes, R. F. Haglund Jr., and L. C. Feldman, "Switchable reflectivity on silicon from a composite VO_2-SiO_2 protecting layer," *Applied Physics Letters*, vol. 85, no. 8, pp. 1410–1412, 2004.

[9] A. A. Bugayev and M. C. Gupta, "Femtosecond holographic interferometry for studies of semiconductor ablation using vanadium dioxide film," *Optics Letters*, vol. 28, no. 16, pp. 1463–1465, 2003.

[10] A. Cavalleri, C. Tóth, C. W. Siders et al., "Femtosecond structural dynamics in VO_2 during an ultrafast solid-solid phase transition," *Physical Review Letters*, vol. 87, Article ID 237401, 2001.

[11] D. Ruzmetov, G. Gopalakrishnan, J. Deng, V. Narayanamurti, and S. Ramanathan, "Electrical triggering of metal-insulator transition in nanoscale vanadium oxide junctions," *Journal of Applied Physics*, vol. 106, no. 8, Article ID 083702, 2009.

[12] M. J. Dicken, K. Aydin, I. M. Pryce et al., "Frequency tunable near-infrared metamaterials based on VO_2 phase transition," *Optics Express*, vol. 17, no. 20, pp. 18330–18339, 2009.

[13] T. Driscoll, H.-T. Kim, B.-G. Chae, M. Di Ventra, and D. N. Basov, "Phase-transition driven memristive system," *Applied Physics Letters*, vol. 95, no. 4, Article ID 043503, 2009.

[14] D. Ruzmetov, G. Gopalakrishnan, C. Ko, V. Narayanamurti, and S. Ramanathan, "Three-terminal field effect devices utilizing thin film vanadium oxide as the channel layer," *Journal of Applied Physics*, vol. 107, no. 11, Article ID 114516, 2010.

[15] Q. Gu, A. Falk, J. Q. Wu, L. Ouyang, and H. Park, "Current-driven phase oscillation and domain-wall propagation in $W_xv_{1-x}O_2$ nanobeams," *Nano Letters*, vol. 7, no. 2, pp. 363–366, 2007.

[16] B.-J. Kim, Y. W. Lee, B.-G. Chae et al., "Temperature dependence of the first-order metal-insulator transition in VO_2 and programmable critical temperature sensor," *Applied Physics Letters*, vol. 90, no. 2, Article ID 023515, 2007.

[17] R. M. Briggs, I. M. Pryce, and H. A. Atwater, "Compact silicon photonic waveguide modulator based on the vanadium dioxide metal-insulator phase transition," *Optics Express*, vol. 18, no. 11, pp. 11192–11201, 2010.

[18] J. Cao, W. Fan, Q. Zhou et al., "Colossal thermal-mechanical actuation via phase transition in single-crystal VO_2 microcantilevers," *Journal of Applied Physics*, vol. 108, no. 8, Article ID 083538, 2010.

[19] H. Guo, M. I. Khan, C. Cheng et al., "VO_2 nanowire-based microthermometer for quantitative evaluation of electron beam heating," *Nature Communications*, vol. 5, pp. 1–5, 2014.

[20] C. Cheng, D. Fu, K. Liu et al., "Directly metering light absorption and heat transfer in single nanowires using metal-insulator transition in VO_2," *Advanced Optical Materials*, vol. 3, no. 3, pp. 336–341, 2015.

[21] S. J. Chang, J. B. Park, G. Lee et al., "In situ probing of doping- and stress-mediated phase transitions in a single-crystalline VO_2 nanobeam by spatially resolved Raman spectroscopy," *Nanoscale*, vol. 6, no. 14, pp. 8068–8074, 2014.

[22] L. Whittaker, C. J. Patridge, and S. Banerjee, "Microscopic and nanoscale perspective of the metal-insulator phase transitions of VO_2: some new twists to an old tale," *Journal of Physical Chemistry Letters*, vol. 2, no. 7, pp. 745–758, 2011.

[23] Y. Wu, L. Fan, W. Huang et al., "Depressed transition temperature of $W_xV_{1-x}O_2$: mechanistic insights from the X-ray absorption fine structure (XAFS) spectroscopy," *Physical Chemistry Chemical Physics*, vol. 16, no. 33, pp. 17705–17714, 2014.

[24] M. H. Kim, B. Lee, S. Lee et al., "Growth of metal oxide nanowires from supercooled liquid nanodroplets," *Nano Letters*, vol. 9, no. 12, pp. 4138–4146, 2009.

[25] E. Strelcov, A. V. Davydov, U. Lanke, C. Watts, and A. Kolmakov, "*In situ* monitoring of the growth, intermediate phase transformations and templating of single crystal VO_2 nanowires and nanoplatelets," *ACS Nano*, vol. 5, no. 4, pp. 3373–3384, 2011.

[26] I. S. Kim and L. J. Lauhon, "Increased yield and uniformity of vanadium dioxide nanobeam growth via two-step physical vapor transport process," *Crystal Growth and Design*, vol. 12, no. 3, pp. 1383–1387, 2012.

[27] B. S. Guiton, Q. Gu, A. L. Prieto, M. S. Gudiksen, and H. Park, "Single-crystalline vanadium dioxide nanowires with rectangular cross sections," *Journal of the American Chemical Society*, vol. 127, no. 2, pp. 498–499, 2005.

[28] C. Cheng, H. Guo, A. Amini et al., "Self-assembly and horizontal orientation growth of VO_2 nanowires," *Scientific Reports*, vol. 4, pp. 1–5, 2014.

[29] J. I. Sohn, H. J. Joo, A. E. Porter et al., "Direct observation of the structural component of the metal-insulator phase transition and growth habits of epitaxially grown VO_2 nanowires," *Nano Letters*, vol. 7, no. 6, pp. 1570–1574, 2007.

[30] E. Strelcov, A. Tselev, I. Ivanov et al., "Doping-based stabilization of the M2 phase in free-standing VO_2 nanostructures at room temperature," *Nano Letters*, vol. 12, no. 12, pp. 6198–6205, 2012.

[31] S. Lee, C. Cheng, H. Guo et al., "Axially engineered metal-insulator phase transition by graded doping VO_2 nanowires," *Journal of the American Chemical Society*, vol. 135, no. 12, pp. 4850–4855, 2013.

[32] J. Wei, H. Ji, W. Guo, A. H. Nevidomskyy, and D. Natelson, "Hydrogen stabilization of metallic vanadium dioxide in single-crystal nanobeams," *Nature Nanotechnology*, vol. 7, no. 6, pp. 357–362, 2012.

[33] J. Wu, Q. Gu, B. S. Guiton, N. P. de Leon, L. Ouyang, and H. Park, "Strain-induced self organization of metal-insulator domains in single-crystalline VO_2 nanobeams," *Nano Letters*, vol. 6, no. 10, pp. 2313–2317, 2006.

[34] J. I. Sohn, H. J. Joo, D. Ahn et al., "Surface-stress-induced Mott transition and nature of associated spatial phase transition in single crystalline VO_2 nanowires," *Nano Letters*, vol. 9, no. 10, pp. 3392–3397, 2009.

[35] J. I. Sohn, H. J. Joo, K. S. Kim et al., "Stress-induced domain dynamics and phase transitions in epitaxially grown VO_2 nanowires," *Nanotechnology*, vol. 23, no. 20, Article ID 205707, 2012.

[36] J. Cao, E. Ertekin, V. Srinivasan et al., "Strain engineering and one-dimensional organization of metal–insulator domains in single-crystal vanadium dioxide beams," *Nature Nanotechnology*, vol. 4, no. 11, pp. 732–737, 2009.

[37] J. M. Atkin, S. Berweger, E. K. Chavez et al., "Strain and temperature dependence of the insulating phases of VO_2 near the metal-insulator transition," *Physical Review B—Condensed Matter and Materials Physics*, vol. 85, no. 2, Article ID 020101, 2012.

[38] S. Zhang, I. S. Kim, and L. J. Lauhon, "Stoichiometry engineering of monoclinic to rutile phase transition in suspended single crystalline vanadium dioxide nanobeams," *Nano Letters*, vol. 11, no. 4, pp. 1443–1447, 2011.

[39] W.-K. Hong, J. B. Park, J. Yoon et al., "Hydrogen-induced morphotropic phase transformation of single-crystalline vanadium dioxide nanobeams," *Nano Letters*, vol. 13, no. 4, pp. 1822–1828, 2013.

[40] E. Strelcov, Y. Lilach, and A. Kolmakov, "Gas sensor based on metal-insulator transition in VO_2 nanowire thermistor," *Nano Letters*, vol. 9, no. 6, pp. 2322–2326, 2009.

[41] B. Hu, Y. Ding, W. Chen et al., "External-strain induced insulating phase transition in VO_2 nanobeam and its application as flexible strain sensor," *Advanced Materials*, vol. 22, no. 45, pp. 5134–5139, 2010.

[42] B. Hu, Y. Zhang, W. Chen, C. Xu, and Z. L. Wang, "Self-heating and external strain coupling induced phase transition of VO_2 nanobeam as single domain switch," *Advanced Materials*, vol. 23, no. 31, pp. 3536–3541, 2011.

[43] R. Xie, C. T. Bui, B. Varghese et al., "An electrically tuned solid-state thermal memory based on metal-insulator transition of single-crystalline VO_2 nanobeams," *Advanced Functional Materials*, vol. 21, no. 9, pp. 1602–1607, 2011.

[44] S.-H. Bae, S. Lee, H. Koo et al., "The memristive properties of a single VO_2 nanowire with switching controlled by self-heating," *Advanced Materials*, vol. 25, no. 36, pp. 5098–5103, 2013.

[45] J. Cao, Y. Gu, W. Fan et al., "Extended mapping and exploration of the vanadium dioxide stress-temperature phase diagram," *Nano Letters*, vol. 10, no. 7, pp. 2667–2673, 2010.

[46] S. Zhang, J. Y. Chou, and L. J. Lauhon, "Direct correlation of structural domain formation with the metal insulator transition in a VO_2 nanobeam," *Nano Letters*, vol. 9, no. 12, pp. 4527–4532, 2009.

[47] A. C. Jones, S. Berweger, J. Wei, D. Cobden, and M. B. Raschke, "Nano-optical investigations of the metal-insulator phase behavior of individual VO_2 microcrystals," *Nano Letters*, vol. 10, no. 5, pp. 1574–1581, 2010.

[48] N. B. Aetukuri, A. X. Gray, M. Drouard et al., "Control of the metal-insulator transition in vanadium dioxide by modifying orbital occupancy," *Nature Physics*, vol. 9, no. 10, pp. 661–666, 2013.

[49] C. Miller, M. Triplett, J. Lammatao et al., "Unusually long free carrier lifetime and metal-insulator band offset in vanadium dioxide," *Physical Review B*, vol. 85, no. 8, Article ID 085111, 2012.

[50] Y. Cheng, T. Zhang, Y. Cai, K. M. Ho, K. K. Fung, and N. Wang, "Structure and metal-to-insulator transition of VO_2 nanowires grown on sapphire substrates," *European Journal of Inorganic Chemistry*, vol. 2010, no. 27, pp. 4332–4338, 2010.

[51] H. Guo, K. Wang, Y. Deng et al., "Nanomechanical actuation from phase transitions in individual VO_2 micro-beams," *Applied Physics Letters*, vol. 102, no. 23, Article ID 231909, 2013.

[52] C. H. Griffiths and H. K. Eastwood, "Influence of stoichiometry on the metal-semiconductor transition in vanadium dioxide," *Journal of Applied Physics*, vol. 45, no. 5, pp. 2201–2206, 1974.

[53] C. Ko, Z. Yang, and S. Ramanathan, "Work function of vanadium dioxide thin films across the metal-insulator transition and the role of surface nonstoichiometry," *ACS Applied Materials and Interfaces*, vol. 3, no. 9, pp. 3396–3401, 2011.

[54] E. Hryha, E. Rutqvist, and L. Nyborg, "Stoichiometric vanadium oxides studied by XPS," *Surface and Interface Analysis*, vol. 44, no. 8, pp. 1022–1025, 2012.

[55] C. Clavero, J. L. Slack, and A. Anders, "Size and composition-controlled fabrication of thermochromic metal oxide nanocrystals," *Journal of Physics D: Applied Physics*, vol. 46, no. 36, Article ID 362001, 2013.

[56] A. Simo, B. Mwakikunga, B. T. Sone, B. Julies, R. Madjoe, and M. Maaza, "VO_2 nanostructures based chemiresistors for low power energy consumption hydrogen sensing," *International Journal of Hydrogen Energy*, vol. 39, no. 15, pp. 8147–8157, 2014.

[57] K. J. Choi and H. W. Jang, "One-dimensional oxide nanostructures as gas-sensing materials: review and issues," *Sensors*, vol. 10, no. 4, pp. 4083–4099, 2010.